Meetings in Physics at University of Sofia, vol. 5
ed. A. Proykova, Heron Press, Sofia, 2004

DIFFUSION-CONTROLLED INDUCTIVE DISCHARGES

St. Kolev,[1] A. Shivarova[1] and Kh. Tarnev[2]

[1]Department of Radiophysics and Electronics, Faculty of Physics, Sofia University, 1164 Sofia, Bulgaria
[2]Department of Applied Physics, Technical University of Sofia, 1000 Sofia, Bulgaria

Abstract. A self-consistent model of diffusion-controlled inductive discharges in an argon gas is presented. The structure of the discharge, composed out of plasma- and wave- characteristics, and its modifications with varying gas pressure and applied power are discussed.

1 Introduction

The inductive discharges are well-known with their numerous applications to spectra-chemical analysis and crystal growth, started many years ago with discharges at high gas pressure as well as to surface processing, plasma chemistry, light sources and ion sources developed recently with low-pressure discharges.

Plasma production in a straight cylindrical tube positioned inside a coil (solenoid) is the classical form of inductive discharges. The discharge operation is in a H-mode, i.e. as an inductive discharge, when the applied power is high enough. Than the discharge maintenance is in the azimuthal electric field induced by an axial magnetic field, produced by the current in the coil.

The wide use of the inductive discharges stimulates the extended research on their modelling (see, e.g. [1-4]). However, the fluid-plasma models of diffusion-controlled discharges in the literature are still in the limits of the Schottky approximation [5], and in spite of the high plasma density production in the inductive discharges the nonlinear processes of step ionization and recombination are ignored.

Based on recent understanding on self-consistent modelling of surface-wave-sustained discharges [6,7], which shows the importance of accounting for the nonlinear processes of step ionization and recombination, the study presents a fluid-plasma model of inductive discharges sustained in an argon in the gas pressure range of the diffusion regime. The self-consistent structure of the discharge composed out of plasma- and wave- characteristics and its modifications with varying gas pressure p and applied power P are discussed.

2 Discharge model

Inductive discharges sustained in an argon in the gas-pressure range of the diffusion-controlled regime are described within the fluid-plasma theory. With a length L of the coil and, respectively, of the discharge larger than the radius R of the gas discharge tube, the edge effects can be neglected. Thus, the model is one-dimensional, with axial magnetic (H_z) and azimuthal electric (E_φ) fields completing the field configuration.

The gas-discharge part of the model consist of:

• the relation between power Θ absorbed on average by an electron and plasma density n averaged over the discharge cross section [7]

$$\frac{\Theta}{\Theta_i} = \left[\frac{\left(\frac{\mu}{R}\right)^2 D_A + \tilde{\mu}\rho_r \overline{n}}{\nu_i^0 + \tilde{\mu}\frac{\rho_{si}^0 \overline{n}}{1+\tilde{\mu}\eta\overline{n}}} \right]^{1/s} \qquad (1)$$

derived from the particle-balance and electron-energy-

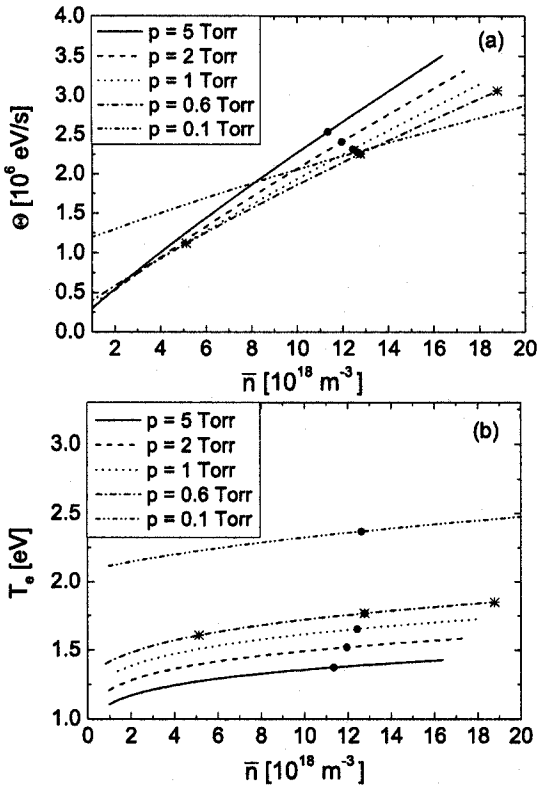

Figure 1. Relation of $\overline{n}$ to Θ [in (a)] and T_e [in (b)] for different values of p. By circles and stars, the positions on the curves of the discharges discussed in Section 3 for P = const. and varying p as well as for p = const. and varying P, are marked.

balance equations,

- the expression for the total power P sustaining the discharge

$$P = \pi R^2 \overline{n} \Theta L \tag{2}$$

and

- the Bohm criterion

$$\frac{v_s}{D_A} = \frac{\mu}{R} \frac{J_1(\mu)}{J_0(\mu)} \tag{3}$$

applied at the boundary between the plasma and the wall sheath, with a thickness of the sheath tending to zero. The latter relation determinates the parameter μ of the radial inhomogeneity of the plasma density of the Bessel-type of radial profile obtained

$$n(r) = n(r=0) J_0(\mu r/R). \tag{4}$$

The electron temperature T_e is related to the power Θ according to:

$$T_e = -\frac{U_\star}{\ln \Theta/\Theta_i} \tag{5}$$

obtained from the electron-energy balance considered in a nonlocal approach.

In (1)–(5), D_A is the ambipolar diffusion coefficient, ρ_r is the recombination coefficient, $\Theta_i = \nu_\star^0 U_\star$, $\nu_\star^0$, ν_i^0 and ρ_{si}^0, depending on p, are the slowly varying functions of T_e [6,7] which enter the frequencies of excitation $\nu_\star = \nu_\star^0 \exp(-U_\star/T_e)$ and direct ionization $\nu_i = \nu_i^0 \exp(-U_i/T_e)$ as well as the rate coefficient $\rho_{si} = \rho_{si}^0 \exp(-U_i/T_e)$ of step ionization; η describes the saturation of the step ionization and $U_\star$ and U_i are, respectively, the energies of excitation of the first excited atom state and of ionization. The other notation is as follows: $\widetilde{\mu} = \mu/2J_1(\mu)$, J_0 and J_1 are the Bessel functions and v_s is the ion sound velocity.

Figure 1 presents the relation of $\overline{n}$ to Θ and T_e, respectively, in (a) and (b), in a $\overline{n}$-range, typical for inductive discharges. With the high plasma-density production in these discharges, the discharge maintenance is on that branch [6,7] of the (Θ-$\overline{n}$)-relation which is determined by strong impact of saturated step ionization and recombination: Θ increases with the $\overline{n}$-increase because of increasing recombination losses. (The Schottky approximation $\nu_i = (\mu/R)^2 D_A$ is for quite lower densities which do not show evidence on the (Θ-$\overline{n}$)-curves in Figure 1(a).) The crossing of the (Θ-$\overline{n}$)-curves for different p (Figire 1(a)) is due to the influence of the recombination. In spite of the nonmonotonic behaviour of Θ for different p-values, T_e - being determined by Θ/Θ_i where Θ_i is proportional to p - monotonically decreases with increasing p (Figure 1(b)).

The electrodynamical part of the model is completed by the wave field equation for radially-inhomogeneous

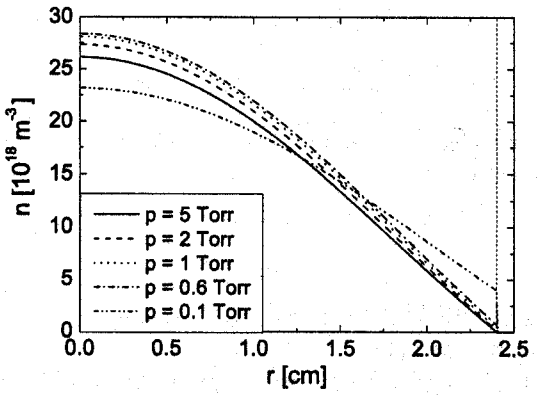

Figure 2. Radial profiles of the plasma density for different p-values and $P = 500$ W.

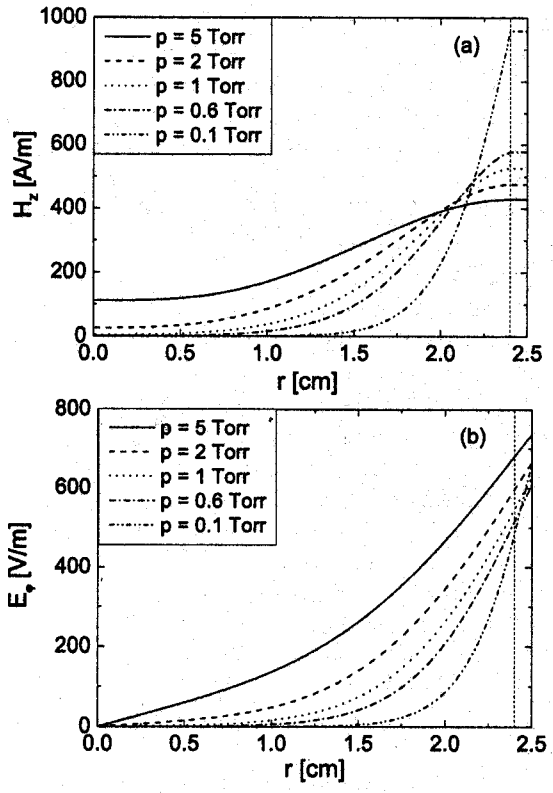

Figure 3. Radial profiles of the H_z [in (a)] and E_φ [in (b)] field amplitudes for different p-values and $P = 500$ W.

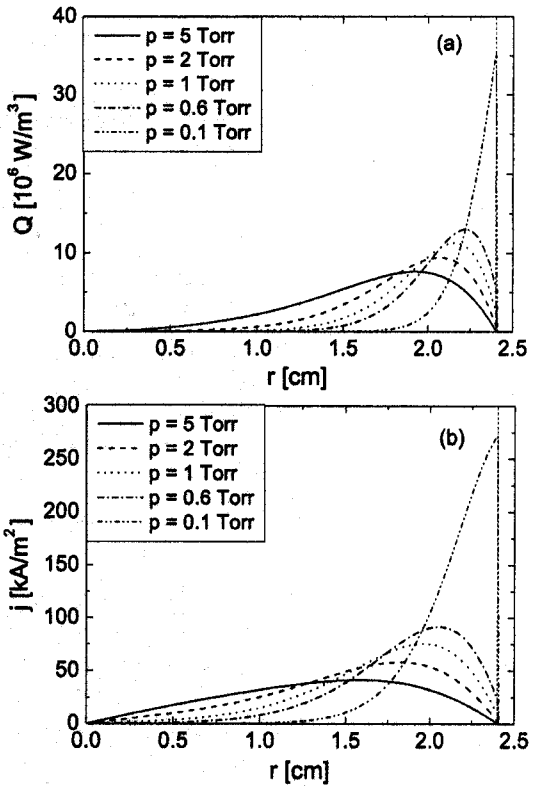

Figure 4. Radial profiles of the absorbed power Q and current density j_φ for different p-values and $P = 500$ W.

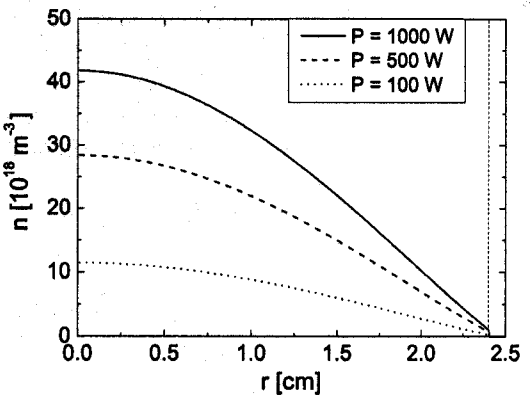

Figure 5. The same as in Figure 2 but for p = const. and different P-values.

plasmas

$$\frac{\mathrm{d}^2 H_z(r)}{\mathrm{d}r^2} + \frac{1}{r}\frac{\mathrm{d}H_z(r)}{\mathrm{d}r} - \frac{1}{\varepsilon(r)}\frac{\mathrm{d}\varepsilon(r)}{\mathrm{d}r}\frac{\mathrm{d}H_z(r)}{\mathrm{d}r} + \frac{\omega^2}{c^2}\varepsilon(r)H_z(r) = 0 \qquad (6)$$

and the relation of E_φ to H_z

$$E_\varphi = -\frac{\mathrm{i}}{\omega\varepsilon_0\varepsilon}\frac{\mathrm{d}H_z}{\mathrm{d}r}, \qquad (7)$$

both steaming from the Maxwell equations. Here ω is the rf-frequency (the frequency of the transverse bulk wave sustaining the discharge), ε_0 and c are respectively, the vacuum permittivity and the light speed in vacuum and $\varepsilon = 1 - [\omega_p^2(r)/\omega(\omega + \mathrm{i}\nu)]$ with ω_p and ν being, respectively, the plasma frequency and the electron-neutral elastic collision frequency, is the plasma permittivity.

In the numerical procedure first the set (1)–(5) is solved in iteration (with respect to T_e) and then eqs. (6) and (7) are solved with $(\mathrm{d}H_z/\mathrm{d}r)|_{r=0} = 0$ and a $H_z(r = 0)$-value which satisfies the condition $Q_{total} \equiv (1/2)\int_{(\mathrm{V})} \sigma_r |E_\varphi|^2 \mathrm{d}V = P$ where Q is the absorbed power and σ_r is the real part of the plasma conductivity. The wall thickness is taken into account in calculating the radial field profiles.

3 Results on the discharge structure

The results for Θ, T_e and $\overline{n}$, presented in Figure 1, together with the radial profiles of plasma density $n(r)$, field intensities $H_z(r)$ and $E_\varphi(r)$, absorbed power $Q(r)$ and current density $j_\varphi(r)$ (Figures 2–7) complete the total self-consistent structure of the discharges. Argon discharges sustained at frequency $f \equiv \omega/2\pi = 27$ MHz in a quartz tube (with permittivity 3.78 and inner and external radii $R = 2.4$ cm and $R = 2.5$ cm, respectively) are considered for constant gas temperature ($T_g = 600$ K); the length of the coil is $L = 6$ cm. The position $R = 2.4$ cm is marked by a dash line in Figures 2–7. In the gas-pressure range studied [$p = (0.1 - 5)$ Torr], the (ν/ω)-ratio varies in the interval (ν/ω) =0.56–13, and, thus, the discharge maintenance is under the conditions of strong collisions.

Figures 2–4 show the modifications of the radial profiles of the plasma- and wave-characteristics with the gas

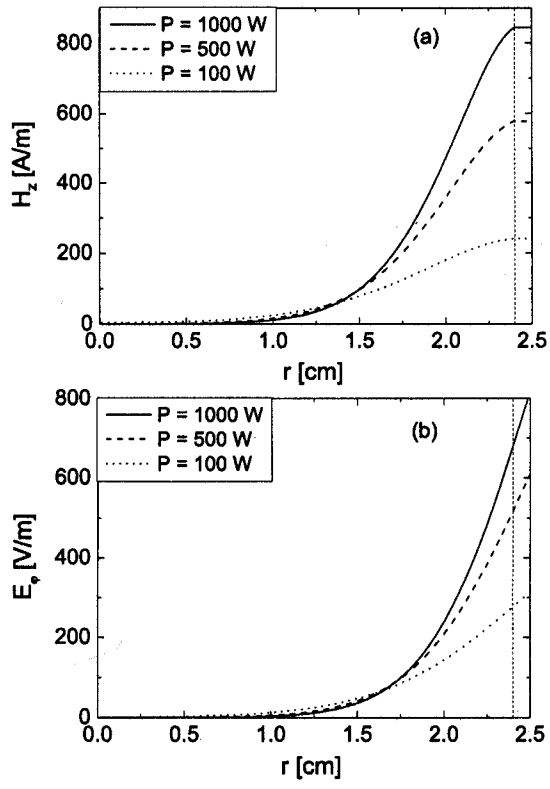

Figure 6. The same as in Figure 3 but for p = const. and different P-values.

pressure increase. With respect to the plasma behaviour, the value of $p = 0.6$ Torr appears to be the most efficient: For a given applied power the discharge is with the highest plasma density. Although $\overline{n}$ for $p = 0.1$ Torr is not too much lower than the $\overline{n}$-values for $p \geq 1$ Torr (Figure 1(a)), the $n(r)$-profile for $p = 0.1$ Torr differs quite a lot from those for $p \geq 0.6$ Torr. This is due to the low value of μ obtained ($\mu = 2.089$) for $p = 0.1$ Torr compared to the μ-values for $p \geq 0.6$ Torr [$\mu \in (2.355 - 2.3995)$]. In general, μ increases with p. With the gas-pressure increase, the field penetration inside the plasma increases (Figure 3): At low pressure ($p = 0.1$ Torr) the skin depth is 0.23 cm and the field is concentrated close to the wall whereas at high pressure ($p = 5$ Torr) the skin depth increases to 0.83 cm. With the plasma density drop (Figure 2) and the increase of

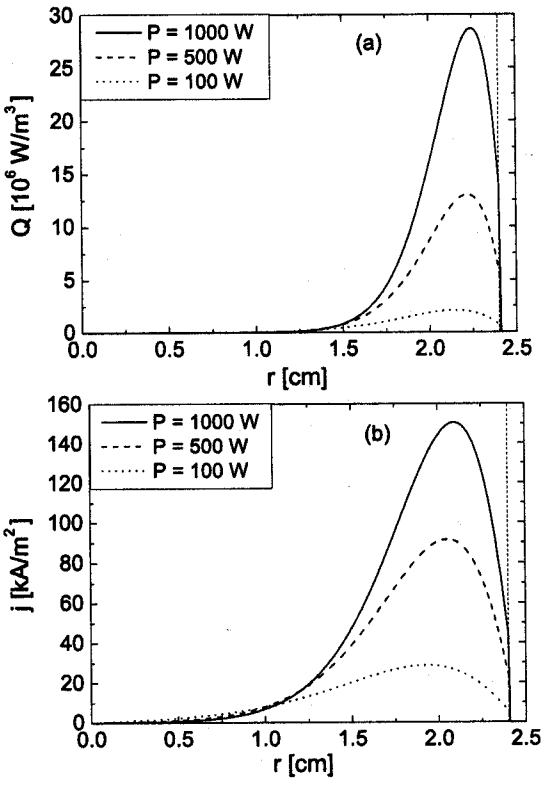

Figure 7. The same as in Figure 4 but for p = const. and different P-values.

the E_φ-field (Figure 3(b)) towards the discharge wall, both $Q = (1/2)\sigma_r|E_\varphi|^2$ and $j_\varphi = \sigma_r|E_\varphi|$ have maxima (Figire 4). Due to the behaviour of the radial E_φ-profiles (Figure 3(b)), these maxima shift - with p - towards the discharge axis. Since $Q \propto |E_\varphi|^2$ and $j_\varphi \propto |E_\varphi|$, the maxima of Q are closer to the wall. Although Q_{total} obtained after integration of $Q(r)$ over the discharge cross section stays constant ($Q_{total} = P$), because of the decrease of σ_r with the p-increase ($\sigma_r \propto \overline{n}/\nu$) the lower-pressure discharges need higher $\overline{E}_\varphi$ for their maintenance.

Figures 5–7 show changes of the radial profiles of the discharge characteristics with increasing P for constant p. The plasma density (Figures 1 and 5) and the field intensity (Figure 6) increase with P; μ stays almost constant ($\mu \cong 2.35$). The power deposition (Figure 7(a)) and the plasma current (Figure 7(b)) are concentrated close to the wall with maxima which slightly shift - with the P-decrease - towards the discharge axis. Again, the maxima of j_φ are shifted towards the discharge axis with respect to those of Q. The skin depth decreases from 0.52 cm to 0.35 cm with the P-increase from 100 to 1000 W.

4 Conclusion

The study presents a self-consistent model of the diffusion-controlled regime of inductive discharges in an argon gas. The extension of the work will be towards modelling of low-pressure inductive discharges in hydrogen regarding their use as sources of negative ions in fusion devices.

Acknowledgments

The work is within RTD Shared Cost Project FU06-CT-00139 of the EURATOM programme.

References

[1] M. A. Lieberman and A. J. Lichtenberg (1994) *Principles of Plasma Discharges and Material processing*, N.Y., Wiley.

[2] J. Denneman (1990) *J. Phys. D: Appl. Phys.* **23**, 293.

[3] G. Lister and M. Cox (1992) *Plasma Sources Sci. Technol.* **1**, 67.

[4] U. Kortshagen (1996) *J. Phys. D: Appl. Phys.* **29**, 1224.

[5] W. Schottky (1924) *Phys. Z.* **25**, 635.

[6] Yu. M. Aliev, H. Schlüter and A. Shivarova (2000) *Guided-Wave-Produced Plasmas*, Berlin, Springer.

[7] K. Makasheva and A. Shivarova (2001) *Phys. Plasmas* **8**, 836.